Journal of Digital Imaging

Clinical Potential of Digital Linear Tomosynthesis Imaging of Total Joint Arthroplasty

Tsutomu Gomi,[1] and Hiroshi Hirano[2]

The present study was performed to evaluate the potential for clinical application of digital linear tomosynthesis in imaging hip prostheses. Volumetric x-ray digital linear tomosysnthesis was used to image hip prostheses. The tomosynthesis was compared to metal artifact reduction (MAR) computed tomography (CT), and non-MAR CT scans of a prosthesis case. The effectiveness of this method in enhancing visibility of a prosthesis case was quantified in terms of the signal-to-noise ratio (SNR), and removal of ghosting artifacts in a prosthesis case was quantified in terms of the artifact spread function (ASF). In the near in-focus plane, the contrast is greater in the MAR CT or tomosynthesis relative to the non-MAR CT. The order of ASF performance of the algorithm was as follows: (1) tomosynthesis; (2) MAR-CT; (3) non-MAR CT. The potential usefulness of digital linear tomosynthesis for evaluation of hip prostheses was demonstrated. Further studies are required to determine the ability of digital linear tomosynthesis to quantify the spatial relationships between the metallic components of these devices as well as to identify bony changes with diagnostic consequences.

KEY WORDS: Digital tomosynthesis, total joint arthroplasty

INTRODUCTION

Interest in tomosynthesis and its clinical applications has increased with recent advances in digital x-ray detector technology. Conventional tomography technology provides planar information of an object from its projection images. In tomography, an x-ray tube and an x-ray film receptor move in opposite directions alongside the object. The relative motion of the tube and the film is predetermined based on the location of the in-focus plane.[1] Only one image plane is generated by a scan and multiple scans are needed to provide a sufficient number of planes to cover the selected structure in the object. In contrast, tomosynthesis acquires only one set of discrete x-ray projections, which can be used to reconstruct any plane of the object retrospectively.[2] Tomosynthesis has been investigated in applications, such as angiography, chest imaging, hand joint imaging, pulmonary imaging, dental imaging, and breast imaging.[3–8] Dobbins et al. presented a review of tomosynthesis techniques.[9]

Analogous to geometric tomography, simple backprojection is the most basic tomosynthesis reconstruction method. Unfortunately, backprojection alone leads to significant contrast-reducing tomographic blur from distant structures, imposed upon the reconstructed plane of interest. More sophisticated tomosynthesis reconstruction methods attempt to correct for the overlying tomographic blur and/or poor depth resolution, and include filtered backprojection (FBP),[10–17] iterative deblurring, [18–22] and iterative reconstruction.[22–24]

On the other hand, X-ray computed tomography (CT) has matured over the last three decades, and it now constitutes a powerful tool in medical diagnostics. As a noninvasive imaging technique, the use of CT has become essential, especially

[1]*From the School of Allied Health Sciences, Kitasato University, 1-15-1 Kitasato, Sagamihara, Kanagawa, 228-8555, Japan.*

[2]*From the Department of Radiology, Shinshu University Hospital, 3-1-1 asahi, Matsumoto, Nagano, 390-8621, Japan.*

Correspondence to: Tsutomu Gomi, tel: +81-427789700; fax: +81-427789628; e-mail: gomi@kitasato-u.ac.jp

Online publication 8 June 2007

doi: 10.1007/s10278-007-9040-9

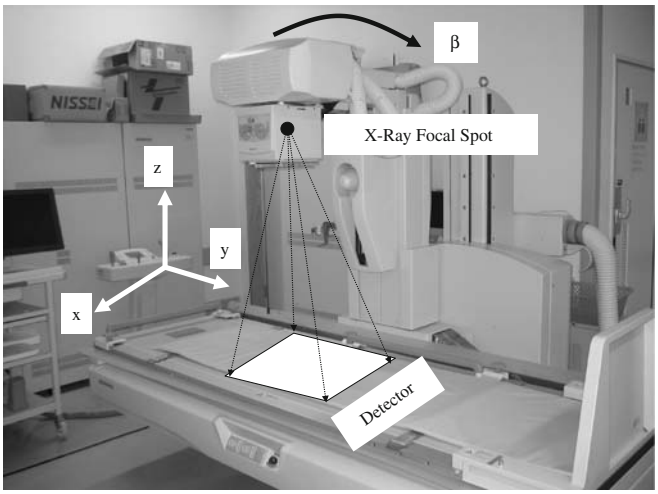

Fig 1. Illustration of a SonialVision Safire tomosynthesis system (Shimadzu Co., Kyoto, Japan). This system acquires 3D projection data by linear motion in the *y*-axis direction (tomographic angle is β degrees). The detector uses a direct conversion-type flat-panel detector (FPD).

since the advent of spiral CT in the 1990s, which led to shorter scan times and improved 3-dimensional (3D) spatial resolution. CT provides high resolution in the tomographic plane, but limited resolution in the axial direction. Therefore, the partial-volume effect may make it difficult to evaluate structures that are not oriented with the direction of the CT tomographic plane. However, the quality of images generated with a CT scanner can still be reduced by the presence of metal objects in the field of view (FOV). Imaging of patients with metal implants such as marker pins, dental fillings, or hip prostheses suffer from artifacts, generally in the form of bright and dark streaks, cupping, and capping; these artifacts are caused mostly by

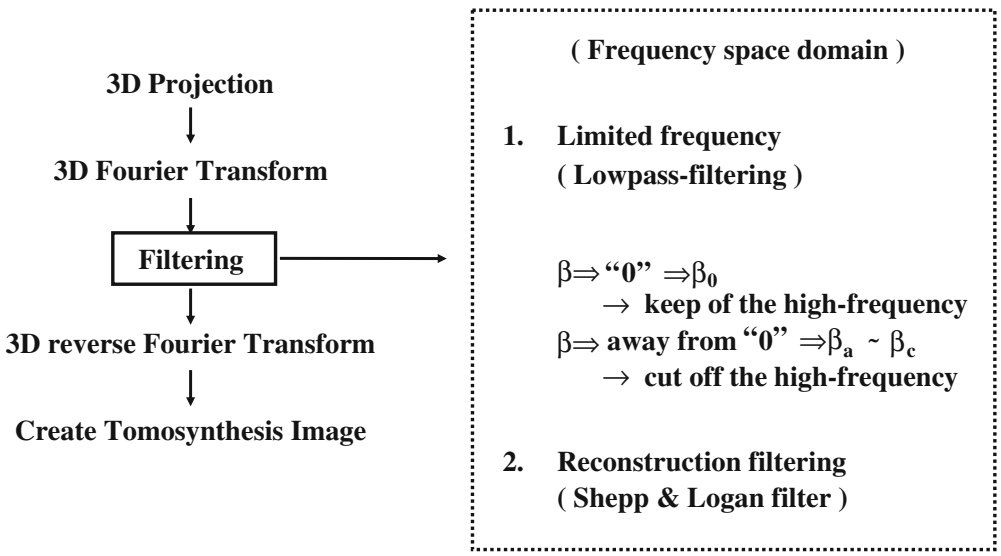

Fig 2. Fourier transform of the 3D volume data generated by backprojection, performing a predetermined filtering process on frequency domain space, which resulted from the 3D Fourier transform, and a 3D reverse Fourier transform of the filtered data in the frequency domain space. The data is then put back to a 3D volume data set. The X-ray tube and flat-panel X-ray detector are first driven to revolve along the circular tracks to scan and pick up images of the region of interest of the object. The operation acquires a group of projection data of the region of interest detected in varied scan positions. Next, the projection data are subjected to a filtering process described below. The filtering process is performed in the Fourier domain space.

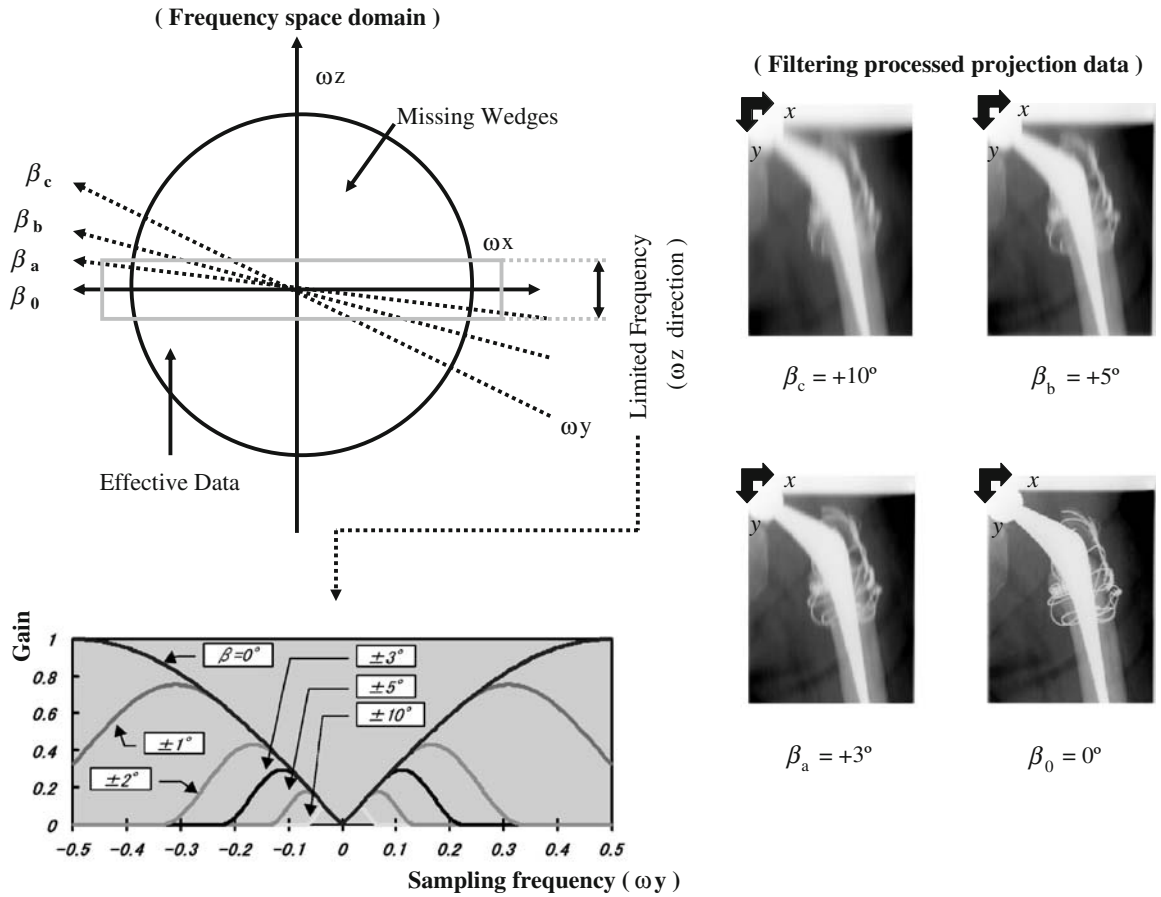

Fig 3. Diagram of constrained tomosynthesis showing how the projections were modified 3D filtered backprojection (FBP). The Fourier domain space low-pass filtering is characterized by applying a low-pass filter in the direction of the sectional axis (ω_z-axis) to lessen the fluence of the data from the missing wedges.

quantum noise, scattered radiation, and beam hardening.[25] Metal artifacts influence image quality by reducing contrast and by obscuring details, thus impairing the detectability of structures of interest; in the worst case, this can make a diagnosis impossible. In addition, CT values are impaired, which can lead to errors in using these data, as for example for attenuation correction in positron emission tomography (PET)/CT.[26] The metallic components of arthroplasty devices are such high-contrast objects, and therefore generate artifacts when imaged using CT scans. These artifacts can make it extremely difficult or impossible to interpret images of these devices. These artifacts, along with the partial-volume effect, severely limit the potential for objective quantification of total joint replacements with CT.

Methods for reduction of metal artifacts aim to improve the quality of images affected by this type of artifacts. In recent years, modified iterative[27–31] or wavelet reconstruction techniques[32] have produced promising results, but these methods cannot be combined with the fast and robust filtered backprojection (FBP) algorithm, which constitutes the standard reconstruction technique implemented in modern CT scanners.

In this report, we focus on the potential application of linear motion digital linear tomosynthesis using a modified FBP[33,34] (Gomi et al., 2006; presented at the annual meeting of the Radiological Society of North America) algorithm for enhanced performance, which is used for imaging of hip prostheses. The present study was performed to evaluate the clinical application of digital linear tomosynthesis in imaging hip prostheses using the relatively new commercial tomosynthesis from Shimadzu SonialVision Safire with a modified FBP algorithm. Tomosynthesis was

compared with metal artifact reduction (MAR) CT and non-MAR CT scans of a hip prosthetic case.

MATERIALS AND METHODS

Tomosynthesis System

To examine the potential usefulness of digital linear tomosynthesis (Fig. 1) in replacing the CT, data were collected using a digital linear tomosynthesis system (SonialVision Safire; Shimadzu Co., Kyoto, Japan). This system consists of an x-ray tube (0.4-mm focal spot) and a 432×432 mm digital flat-panel detector (1,024×1,024 pixels, amorphous selenium) with 421-μm pixel size. The x-ray collimator is shifted during acquisition to conform the x-ray illumination area to the detector. The motion of the collimator is synchronized with the motion of the tube. A data set with 67 projection images and a tomographic angle of 40° was obtained. X-rays of 80 peak kilovoltage (kVp) and 160 mA were used, with an exposure time of 200 ms per view. An antiscatter grid was used. The source to isocenter distance was 980 mm, and the source to detector distance was 1,300 mm. Images were transferred to a personal computer with a 2.4-GHz Intel Xeon CPU, 2,096 MB of RAM, and running Windows 2000 for tomosynthesis reconstruction.

Reconstruction Algorithm

We evaluated the use of the Shimadzu SonialVision Safire reconstruction algorithm (modified FBP[33,34] [Gomi et al., 2006 Radiological Society of North America (RSNA) meeting]) in this study. This modified FBP provides a description of

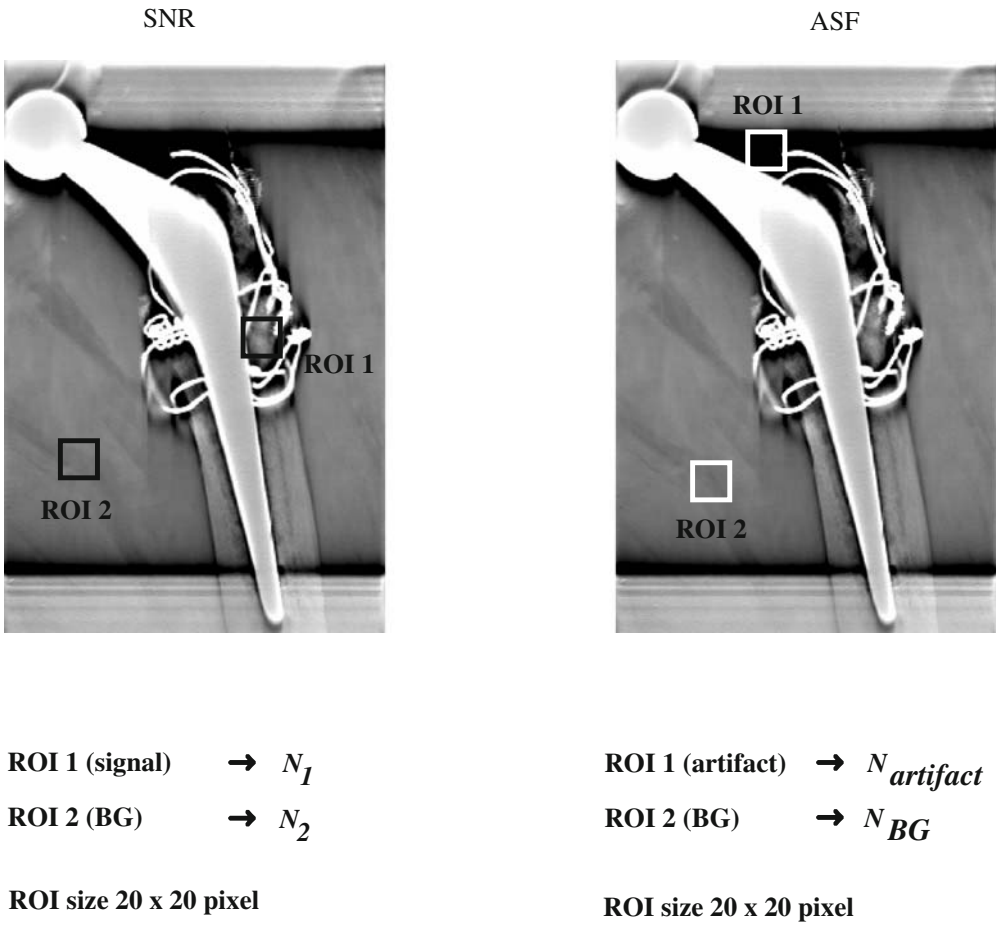

Fig 4. Single projection of prosthetic case. Areas of measurement for the SNR and ASF metric are shown.

filtering that can be used in combination with backprojection to yield tomosynthesis slice images with desired properties (Fig. 2).

Here, we will describe the Fourier domain space low-pass filtering in greater detail. The Fourier domain space low-pass filtering has a Gaussian low-pass filter characteristic as expressed in Figure 3. This low-pass filtering applies a low-pass filter in the direction of the sectional axis (ω_z-axis) of the Fourier domain space data (3D Fourier distribution image). The necessity for this low-pass filtering will be discussed below. The Fourier domain space data having undergone 3D Fourier transform have missing wedges centering on the ω_z-axis, the vertices of which meet at the origin of the Fourier domain space coordinates. The missing wedges are void of data. The missing wedges are different in size (volume) from one row of pixels to another of flat panel detector. That is, the missing wedges have a central angle and volume enlarging in proportion to an angle of inclination of a point-to-point path extending between the center of the cone beam x-rays emitted from the x-ray tube and each of pixel rows arranged in the scan axis (z-axis) of flat panel detector, with respect to a straight line extending from the center point of the cone beam x-rays through the center point of a particular slice of patient to the row of pixels at the center of flat panel detector. These wedges result from the non-CT type radiography in which resolving scans are made about the sectional axis and in the planes opposed to each other across the patient. That is, radiography is carried out without driving the x-ray tube and flat panel detector to make more than a half revolution about the body axis of the patient. This results in low resolution in the direction of the sectional axis (z-axis), thereby generating the "missing wedges." Thus, the Fourier domain space low-pass filtering is characterized by applying a low-pass filter in the direction of the sectional axis (ω_z-axis) to lessen the influence of the data from the missing wedges.

Evaluation of a Signal-to-Noise Ratio (SNR) and Artifact

To demonstrate the potential benefits of digital tomosynthesis compared with CT in imaging hip prostheses, we used one clinical case, a 52-year-old female with total hip arthroplasty. The digital linear tomosynthesis images were reconstructed

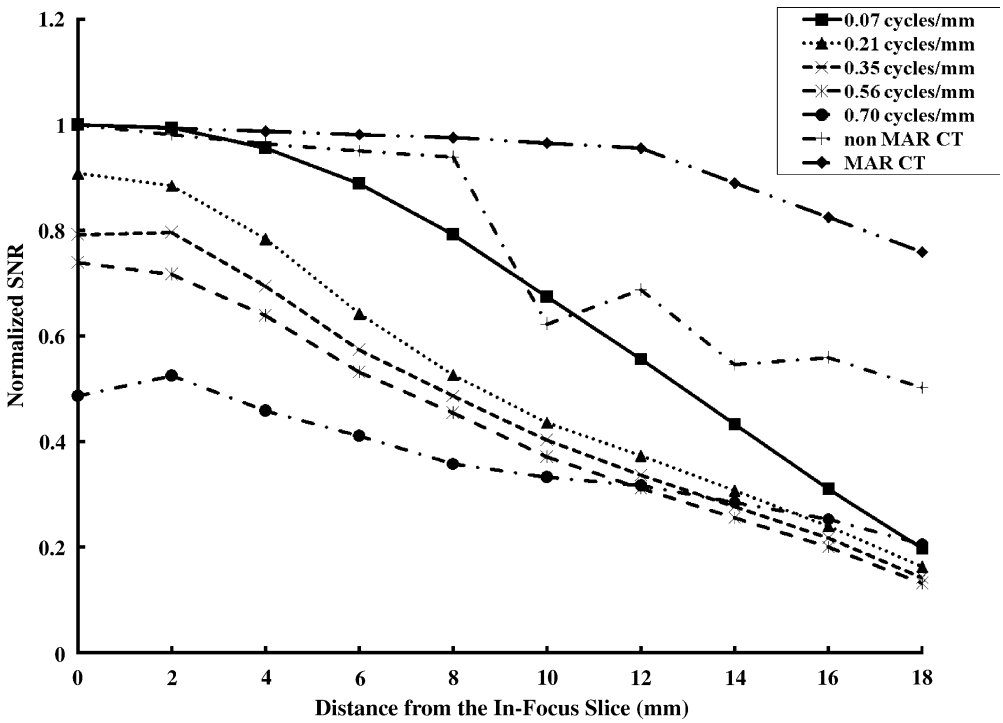

Fig 5. Signal-to-noise ratio (SNR) versus distance from the in-focus plane for each algorithm.

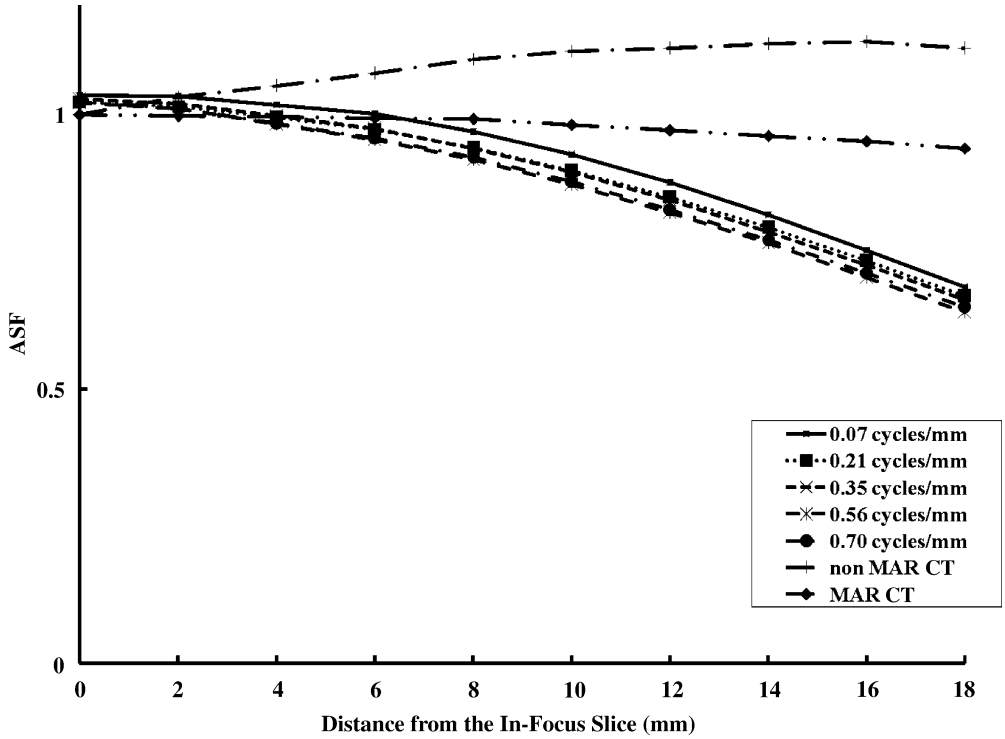

Fig 6. Artifact spread function (ASF) versus distance from the in-focus plane for each algorithm.

using the following parameters: reconstruction interval, 2 mm; limited frequency (Fig. 3), 0.07–0.7 cycles/mm. CT scans were performed on a multislice CT scanner (16-slice LightSpeed scanner; GE Medical Systems, Milwaukee, WI, USA), with 120 kVp, 200 mAs, 0.625 mm×16 collimation, and 0.75-s gantry rotation time (900 views/rotation) at a beam-pitch of 0.93. Multiplanar reformations (MPR) of images (MPR images; 2-mm slice thickness, 2-mm reconstruction interval, 580-μm voxel size) of the CT scan were compared with the tomosynthesis images. MAR processing was performed using the iterative reconstruction algorithm (four subsets, 15 iterations).[31]

The signal-to-noise ratio (SNR) in the prosthetic case was determined. The SNR is defined as $\frac{N_1-N_0}{\sigma_0}$, where N_1 is the mean pixel value in the region of interest (ROI) within the object, N_0 is the mean pixel value in the ROI in a background area, and σ_0 is the standard deviation of pixel values in the background ROI (Fig. 4). Throughout these results, σ_0 includes structure noise that can obscure the object, in addition to photon statistics and electronic noise.

Wu et al. proposed an artifact spread function (ASF) metric to quantify artifacts observed in planes outside the focus image plane.[35] The artifacts are generated from real features located in the focus image plane, and resemble the real feature. The artifacts exhibited in image planes are defined by the ASF as:

$$\mathrm{ASF}(z) = \frac{N_{artifact}(z) - N_{BG}(z)}{N_{artifact}(z_0) - N_{BG}(z_0)},$$

where z_0 is the location of the in-focus plane of the real feature, z is the location of the off-focus plane, and $N_{\mathrm{artifact}}(z_0)$ and $N_{\mathrm{BG}}(z_0)$ are the average pixel intensities of the feature and the image background in the in-focus plane, respectively, $N_{\mathrm{artifact}}(z)$ and $N_{\mathrm{BG}}(z)$ are the average pixel intensities of the artifact and the image background in the off-focus plane, respectively (Fig. 4).

RESULTS

The SNR for tomosynthesis, MAR-CT, and non-MAR CT were investigated, as shown in Figure 5. Tomosynthesis of the clear contrast

Fig 7. Tomosynthesis images of the hip prostheses at different heights at the same level as in Figures 8 and 9 (40° tomographic angle, with 67 views; limited frequency is 0.07 cycles/mm). The top row shows soft-tissue information, and the bottom column shows bone information. The new diagnostic information that could not be acquired in CT images is provided. Reduction of the artifacts in the images obtained with show view. The use of tomosynthesis allowed better visualization of the hip prosthesis caused by the blurring of the anatomic structures above and below the visualized planes. However, in the off-focus plane, the section thickness is too large to result in adequate blurring of overlying structures.

detectability prosthetic case produced an increase in the in-focus plane SNR values, but a reduction in the off-focus plane SNR values. The discrete blur structure shadows in the off-focus plane images were smoothed in the in-focus plane images. In the in-focus plane, the contrast was greater in MAR-CT and tomosynthesis relative to non-MAR CT. In the off-focus plane, the contrast was greater in the MAR-CT and non-MAR CT relative to tomosynthesis. However, tomosynthesis demonstrated its greatest advantages in the modified FBP algorithm.

The chart in Figure 6 presents the ASF results for the prosthetic case. This chart shows the ASF versus the distance from the in-focus slice in millimeters. The number of reconstructed slices was 12. The ASF chart shown in Figure 6 demonstrates that tomosynthesis results in the greatest degree of removal of ghosting artifacts. By examining Figure 5 through the entire thickness of the specimen, the order of ASF performance of the algorithm was as follows: (1) tomosynthesis; (2) MAR-CT; (3) non-MAR CT.

In Figures 5 and 6, the SNR showed a tendency to improve, narrowing the band of limited frequency with variation. The artifacts resulted in a widening of the band of limited frequency with variation. The ASF that yielded little difference with variation over a limited frequency range and the greatest SNR was 0.07 cycles/mm. Therefore, this value was used as the algorithmic optimal cutoff.

As shown in Figure 7, the hip prostheses that lay outside the reconstruction plane were blurred on the digital linear tomosynthesis images. The use of digital linear tomosynthesis improved visualization of the underlying tissue detail by blurring the overlying structures. CT provided information (MPR of images) about the hip prostheses, as shown in Figures 8 and 9. The MPR of CT images suffered from string artifacts in all regions. In addition, because of strong beam hardening and scatter effects, the region of the femur was poorly displayed. The artifacts in the CT images produced by FBP were realistic and resembled actual patient images. The more metal

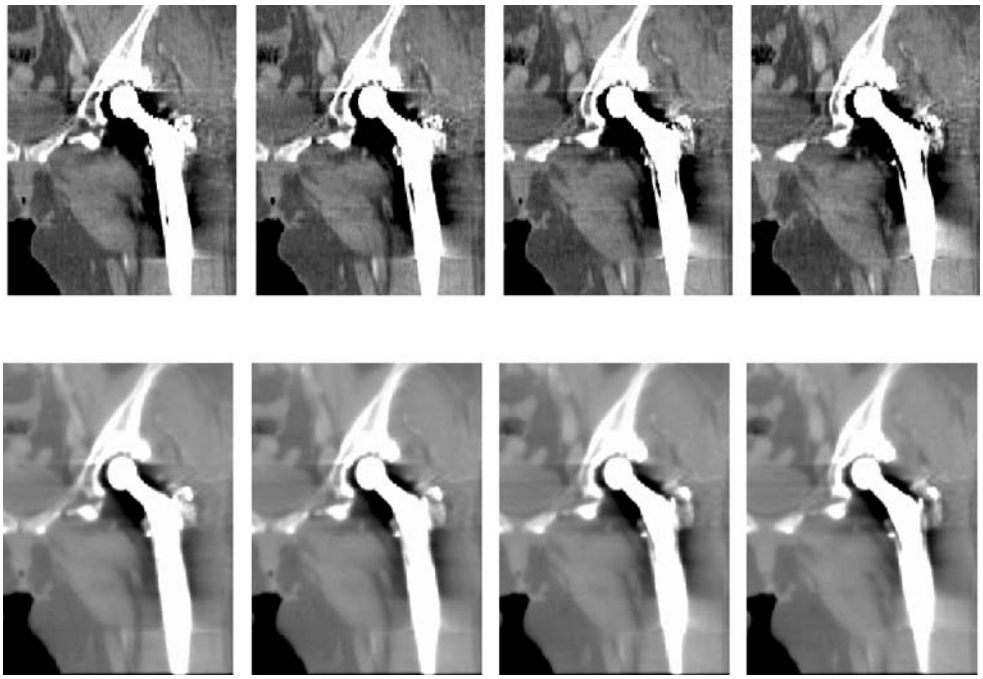

Fig 8. Coronal slice images of the hip prostheses at different heights from MAR-CT and non-MAR CT scan at approximately the same level in Figure 9 (MPR images: 2-mm slice thickness, 2-mm reconstruction interval). The top row shows non-MAR CT images, and the bottom row shows MAR-CT images. Display level (soft tissue information) is a window at 250 HU, window level at 25 HU. Remarkable metal artifacts can be seen occurring in the neighborhood of the hip prosthesis. However, MAR processing reduced the metal artifacts.

present in the field of view (metal backed and bilateral prostheses), the more the metal artifact that was produced. Reconstruction of the incomplete projection data using iterative deblurring produced an essentially metal-artifact-free image for bone and soft tissues and had performance that was superior to the FBP methods. The hip prostheses present on the CT images could be removed effectively by blurring in the 67-projection digital linear tomosynthesis image. This allowed better visualization of the tissue detail directly below the hip prostheses structures.

DISCUSSION

Digital linear tomosynthesis shows adequate overall performance, but its effectiveness depends strongly on the region of the image. Digital linear tomosynthesis images give good results independent of the type of metal present in the patient and show good results for the removal of noise artifacts, especially at greater distances from metal objects. Application of digital linear tomosynthesis to imaging of the hip prostheses appears promising. In addition, the flexibility in the choice of digital linear tomosynthesis imaging parameters based on the desired final images and generated of high-quality images may be beneficial.

Image reconstruction schemes may be selected taking the metric outcome into consideration. MAR-CT with in-focus plane is best for SNR optimization, whereas MAR-CT with off-focus plane is best for SNR optimization. It seems that the number of the projection, total exposure dose, and pixel size of detector are great results in comparison with tomosynthesis. The information contained in a tomosynthesis voxel can be obtained from the 67 projections. Ideally, the number of x-ray quanta for reconstruction of this voxel equals that from a single projection acquired with the same amount of total exposure. Considering the detector noise from the acquisition of each projection, the SNR is reduced in tomosynthesis imaging, which distributes the total exposure over 67 projections. The effect of projection angle, which decreases the photon transmission and reduces the effective detector pixel size, also further reduces the SNR.

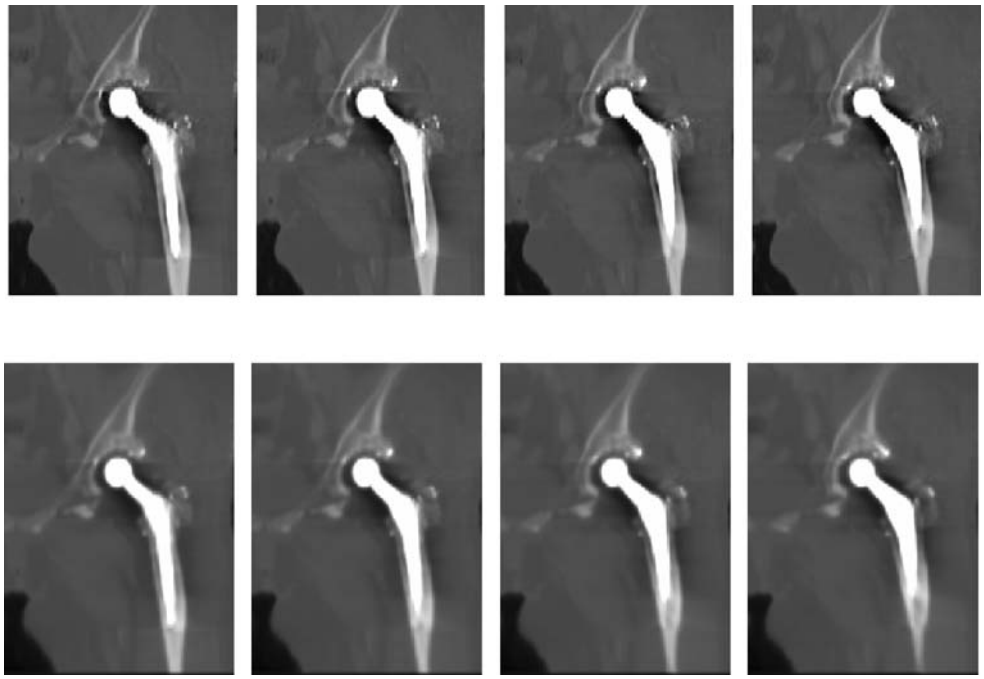

Fig 9. Coronal slice images of the hip prostheses at different heights from MAR-CT and non-MAR CT scans at approximately the same level in Figure 8 (MPR images: 2-mm slice thickness, 2-mm reconstruction interval). The top row shows non-MAR CT images, and the bottom row shows MAR-CT images. Display level (bone information) is the window at 1,000 HU, window level at 300 HU. Remarkable metal artifacts can be seen occurring in the neighborhood of the hip prosthesis.

At a given projection angle, a high-attenuation feature can create artifacts in any voxel along the lines between the x-ray source and the feature pixels in the projection. Artifact reduction becomes more difficult as the size of the high-attenuation feature increases or the distance between the voxel and the high-attenuation feature decreases. The ASF metric gauges the effectiveness of each reconstruction technique for reducing the ghosting artifact in planes outside the focus plane. It is also a measure of the effectiveness of the techniques for reducing ghosts in the focus plane caused by interfering, overlying structures in planes outside the focus plane.

CT images depend on numerous factors, such as size, shape, density, atomic number, and position of the metal objects, patient size, and the shape of the patient's cross-section. Especially for small implants manufactured from relatively light metals (eg, titanium), the impact of beam hardening and scatter effects is low, so that corrupted CT values can be neglected and noise-induced streaking artifacts pose the main problem to image quality. In these cases, digital linear tomosynthesis appears to be a promising approach for the reduction of artifacts stemming from metals with relatively high atomic numbers (Figs. 7, 8 and 9).

The digital tomosynthesis images presented in this report were acquired using a linear motion of the x-ray tube and detector. The type of motion used during data acquisition dictates the type of blurring of off-focal-plane objects in the image. Linear motion blurs objects in one dimension only, which leads to linear streak artifacts caused by high-contrast off-focal-plane objects.

CONCLUSIONS

In summary, use of digital linear tomosynthesis in imaging of hip prostheses appears promising. The results of the hip prosthesis study suggest that digital linear tomosynthesis can improve image quality compared with

conventional radiography by removing overlying structures and providing limited 3D information. In addition, the digital linear tomosynthesis method appears to allow for significant improvement of images corrupted by metal artifacts. Digital linear tomosynthesis provided higher quality images than CT. Tomosynthesis is the best solution for cases in which the high-attenuation feature causing the artifacts can be segmented accurately from the projection.

REFERENCES

1. Ziedses des Plante BG: Eine neue methode zur differenzierung in der roentgenographie (planigraphie). Acta Radiol 13:182–192, 1932
2. Grant DG: Tomosynthesis. A three-dimensional radiographic imaging technique. IEEE Trans Biomed Eng 19:20–28, 1972
3. Stiel G, Stiel L, Klotz E, et al: Digital flashing tomosynthesis: a promising technique for angiographic screening. IEEE Trans Med Imaging 12:314–321, 1993
4. Warp RJ, Godfrey DG, Dobbins JT: Applications of matrix inverse tomosynthesis. Proc SPIE Med Imaging 3977:376–383, 2000
5. Duryea J, Dobbins JT, Lynch JA: Digital tomosynthesis of hand joints for arthritis assessment. Med Phys 30:325–333, 2003
6. Sone S, Kasuga T, Sakai F, et al: Image processing in the digital tomosynthesis for pulmonary imaging. Eur Radiol 5:96–101, 1985
7. Badea C, Kolitsi Z, Pallikarakis N: A 3D imaging system for dental imaging based on digital tomosynthesis and cone beam CT. Proceedings of conference of the International Federation for Medical and Biological Engineering, vol 2, pp 739–741, 2001
8. Niklason L, Christian B, Kopans D, et al: Digital tomosynthesis in breast imaging. Radiology 205:399–406, 1997
9. Dobbins 3rd, JT, Godfrey DJ: Digital x-ray tomosynthesis: Curent state of the art and clinical potential. Phys Med Biol 48:R65–R106, 2003
10. Edholm P, Granlund G, Knutsson H, Peterson C: Ectomography—a new radiographic method for reproducing a selected slice of varying thickness. Acta Radiol 21:433–442, 1980
11. Knutsson HE, Edholm P, Granlund GH, Peterson CU: Ectomography—a new radiographic reconstruction method. 1. Theory and error estimates. IEEE Trans Biomed Eng 27:640–648, 1980
12. Peterson CU, Edholm P, Granlund GH, Knutsson HE: Ectomography—a new radiographic reconstruction method. 2. Computer-simulated experiments. IEEE Trans Biomed Eng 27:649–655, 1980
13. Matsuo H, Iwata A, Horiba I, Suzumura N: 3-Dimensional image reconstruction by digital tomo-synthesis using inverse filtering. IEEE Trans Med Imaging 12:307–313, 1993
14. Badea C, Kolitsi Z, Pallikarakis: Image quality in extend arc filtered digital tomosynthesis. Acta Radiol 42:244–248, 2001
15. Lauritsch G, Harer WH: A theoretical framework for filtered backprojection in tomosynthesis. Proc SPIE 3338: 1127–1137, 1998
16. Stevens GM, Fahrig R, Pelc NJ: Filtered backprojection for modifying the impulse response of circular tomosynthesis. Med Phys 28:372–380, 2001
17. Stevens GM: Volumetric tomographic imaging. PhD thesis 2001
18. Ruttimann UE, Groenhuis RAJ, Webber RL: Restoration of digital multiple tomosynthesis by a constrained iteration method. IEEE Trans Med Imaging 3:141–148, 1984
19. van der Stelt PF, Ruttimann UE, Webber RL: Enhancement of tomosynthesis images in dental radiology. J Dent Res 65:967–973, 1986
20. Engelke W, Ruttimann UE, Tsuchimochi M, Bacher JD: An experimental study of new diagnostic methods for the examination of osseous lesions in the temporomandibular joint. Oral Surg Oral Med Oral Pathol 73:348–359, 1992
21. Webber RL, Underhill HR, Freimanis RL: A controlled evaluation of tuned-aperture computed tomography applied to digital spot mammography. J Digit Imaging 13:90–97, 2000
22. Suryanarayanan S, Karellas A, Vedantham S, Glick SJ, D'Orsi CJ, Baker SP, Webber RL: Comparison of tomosynthesis methods used with digital mammography. Acta Radiol 7:1085–1097, 2000
23. Bleuet P, Guillemaud R, Desbat L, Magnin I: An adapted fan volume sampling scheme for 3-D algebraic reconstruction in linear tomosynthesis. IEEE Trans Nucl Sci 49:2366–2372, 2002
24. Wu T, Stewart A, Stanton M, McCauley T, Phillips W, Kopans DB, Moore RH, Eberhard JW, Opsahl-Ong B, Niklason L, Williams MB: Tomographic mammography using a limited number of low-dose cone-beam projection images. Med Phys 30:365–380, 2003
25. Hsieh J: Image artifacts, causes, and correction. In: Goleman LW, Fowlkes JB Eds. Medical CT and ultrasound, current technology and applications. Madison: Advanced Medical Publishing, 1995, pp 487–518
26. Kamel EM, Burger C, Buck A, et al: Impact of metallic dental implants on CT-based attenuation correction in a combined PET/CT scanner. Eur Radiol 13:724–728, 2003
27. Wang G, Snyder DL, O'Sullivan JA, et al: Iterative debluring for metal artifacts reduction. IEEE Trans Med Imaging 15:657–664, 1996
28. Wang G, Vannier MW, Cheng PC: X-ray cone-beam tomography for metal artifacts reduction and local region reconstruction. Microsc Microanal 5:58–65, 1999
29. Wang G, Frei T, Vannier MW: A fast iterative algorithm for metal artifact reduction in x-ray CT. Acad Radiol 7:607–614, 2000
30. De Man B, Nuyts J, Dupont P, et al: Reduction of metal streak artifacts in x-ray computed tomography using a transmission maximum a posteriori algorithm. IEEE Trans Nucl Sci 47:977–981, 2000
31. Robertson DD, Yuan J, Wang G, Vannier MW: Total hip prosthesis metal-artifact suppression using iterative deblurring reconstruction. J Comput Assist Tomogr 21:293–298, 1997

32. Zhao S, Robertson DD, Wang G, et al: X-ray CT metal artifact reduction using wavelets: an application for imaging total hip prostheses. IEEE Trans Med Imaging 19:1238–1247, 2000

33. Oikawa S: Radiographic Apparatus. 2002; US patent No. US006463116B1

34. Gomi T, Yokoi N, Hirano H: Evaluation of a digital linear tomosynthesis imaging of temporomandibular joint; initial clinical experience and evaluation. Dentomaxillofac Radiol, 2007 (in press)

35. Wu T, Moore RH, Rafferty EA, Kopans DB: A comparison of reconstruction algorithms for breast tomosynthesis. Med Phys 31:2636–2647, 2004